Published in final edited form as:
Clin Cancer Res. 2006 March 1; 12(5): 1431–1440.

Kinetics of metastatic breast cancer cell trafficking in bone

Pushkar A. Phadke[1,*], **Robyn R. Mercer**[6,*], **John F. Harms**[1], **Yujiang Jia**[2], **Andra R. Frost**[1,3,5], **Jennifer L. Jewell**[6], **Karen M. Bussard**[6], **Shakira Nelson**[6], **Cynthia Moore**[1], **John C. Kappes**[2], **Carol V. Gay**[6], **Andrea M. Mastro**[5,6], and **Danny R. Welch**[1,3,4,5]

1 *Departments of Pathology,*

2 *Medicine-Hematology/Oncology,*

3 *Comprehensive Cancer Center,*

4 *Center for Metabolic Bone Disease,*

5 *NFCR-Center for Metastasis Research, University of Alabama at Birmingham, Birmingham, AL and*

6 *Department of Biochemistry and Molecular Biology, Pennsylvania State University, State College, PA.*

Abstract

Purpose—*In vivo* studies have focused on the latter stages of the bone metastatic process (osteolysis), while little is known about earlier events, e.g., arrival, localization, initial colonization. Defining these initial steps may potentially identify critical points susceptible to therapeutic intervention.

Experimental Design—MDA-MB-435 human breast cancer cells engineered with green fluorescent protein (GFP) were injected into the cardiac left ventricle of athymic mice. Femurs were analyzed by fluorescence microscopy, immunohistochemistry, real-time PCR, flow cytometry and histomorphometry at times ranging from 1 hr to 6 wk.

Results—Single cells were found in distal metaphyses at 1 hr post-injection and remained as single cells up to 72 hr. Diaphyseal arrest occurred rarely and few cells remained there after 24 hr. At 1 wk, numerous foci (2–10 cells) were observed, mostly adjacent to osteoblast-like cells. By 2 wk, fewer but larger foci (≥50 cells) were seen. Most bones had a single large mass at 4 wk (originating from a colony or coalescing foci) which extended into the diaphysis by 4–6 wk. Little change (<20%) in osteoblast or osteoclast numbers was observed at 2 wk; but, at 4–6 wk osteoblasts were dramatically reduced (8% of control), while osteoclasts were reduced modestly (to ~60% of control).

Conclusions—Early arrest in metaphysis and minimal retention in diaphysis highlight the importance of local milieu in determining metastatic potential. These results extend the Seed and Soil hypothesis by demonstrating both inter- and intra-tissue differences governing metastasis location. Ours is the first *in vivo* evidence that tumor cells influence not only osteoclasts, as widely believed, but also eliminate functional osteoblasts, thereby restructuring the bone microenvironment to favor osteolysis. The data also explain why bisphosphonates do heal bone despite inhibiting resorption, implying that concurrent strategies that restore osteoblast function are needed to effectively treat osteolytic bone metastases.

Requests for reprints: Danny R. Welch, Ph.D. Department of Pathology, University of Alabama at Birmingham; 1670 University Blvd.; Volker Hall G-019A; Birmingham, AL 35294-0019; Phone: +1-205-934-2961 Fax: +1-205-975-1126; Email: DanWelch@uab.edu; or, Andrea M. Mastro, Ph.D., Department of Biochemistry and Molecular Biology, 231 South Frear, Pennsylvania State University, University Park, PA 16802; Phone: +1-814-863-0152; Fax: +1-814-863-7024; Email: a36@psu.edu..
* Contributed equally to this work

Keywords

breast cancer; metastasis; bone; osteoblast paralysis

Introduction

Breast cancer has a remarkable predilection to colonize bone, with an incidence between 70 and 85% in patients (1–3). At the time of death, metastatic bone disease accounts for the bulk of the tumor burden (4). For women with bone metastases, the complications – severe, often intractable pain, pathological fractures and hypercalcemia – are catastrophic. Despite obvious clinical importance, very little is understood about the fundamental mechanisms responsible for breast cancer metastasis to bone. Research progress has been hampered by the dearth of, and technical difficulties inherent in, the current models.

Most models of metastasis poorly recapitulate the pathogenesis of breast cancer. The ideal model would involve dissemination from an orthotopic site (i.e., mammary fat pad), colonization and osteolysis. None of the currently available human breast xenograft models spread to bone following orthotopic implantation and only one murine model metastasizes to bone from the mammary fat pad (5). Furthermore, most human cell lines do not metastasize to bone in mice regardless of route of injection. The most commonly used model of breast cancer metastasis to bone involves injection of tumor cells into the arterial circulation via the left ventricle of the heart (4,6–8). This route of injection minimizes first-pass filtration through pulmonary capillaries, thereby allowing more cells to reach the bone.

Current methods to detect bone metastases are insufficiently sensitive (e.g., radiography) or are impractical for adequately statistically powered experiments because of costs or labor intensiveness. Radiography can detect osteolytic lesions only after more than half of calcified bone matrix has been degraded (9). Microcomputerized tomography is not widely available, but is likewise of insufficient resolution to recognize single tumor cells. Serial sectioning (which would be required to locate rare single cells) is cost-prohibitive, except for small studies. As a result, experiments have been limited to late events of metastatic bone disease, such as osteolysis. Therefore, antecedent events (i.e., arrival, lodging, intra-osseous trafficking and colonization) have not been studied except by inference.

To overcome some of the technical limitations, more sensitive methods using reporter molecules, such as luciferase (10) or β-galactosidase (LacZ) have recently been described (11–13). Luciferase, while it allows for *in situ* detection of tumor cells in the bone, does not allow for microscopic localization of the cells. Since luminescence depends upon a fully viable cell, use of luciferase is limited *ex vivo*. β-galactosidase is excellent for studies at the histologic level but cannot be used for studies involving intact bone unless the lesions are macroscopic. Diffusion or distribution of substrate into bone is also a complication.

Fluorescent molecules, like enhanced green fluorescent protein (GFP), have also been employed with some success in early detection of bone metastasis (14–16). We recently utilized the GFP-tagged MDA-MB-435 metastatic human breast cancer cell line to reveal formation of osteolytic bone lesions following intracardiac injection in athymic mice (15). Like luciferase, GFP can be used to detect lesions *in situ*, even though the limits of detection are restrictive (~0.5–1 mm). During experiments designed for other purposes, we detected single tumor cells in bone within minutes post-injection. Since, to the best of our knowledge, no one had ever systematically studied the earliest tumor cell-bone interactions (except by serendipitous histologic sections), we decided to utilize the power of GFP to begin addressing early events associated with breast tumor cells that have already disseminated to bone.

It has long been recognized that, once cells arrive in the bone, they alter homeostasis. Turnover of the skeleton is dynamic and continuous throughout embryonic development and adulthood. Calcified bone matrix turns over completely, on average, every decade (17,18). Calcified matrix remodeling involves interplay between osteoblasts (bone forming cells) and osteoclasts (bone resorbing cells). Altering the balance of activities results either in excessive bone deposition (osteopetrosis) or bone loss (osteoporosis). While larger individual bone lesions contain regions that are both osteopetrotic and osteoporotic, most breast cancer bone metastases are net osteolytic. The current paradigm suggests that tumor cells influence osteoclast activity (4,19). Using the GFP model of breast cancer metastasis to bone, we sought to identify key tumor cell-bone cell interactions (and the timing of those interactions) that occur during the pathogenesis of bone metastasis.

Materials and Methods

Cell lines and culture

Metastatic human breast carcinoma cell line, MDA-MB-435 (MDA-435), a generous gift from Dr. Janet Price (University of Texas–M.D. Anderson Cancer Center, Houston), was stably transfected with pEGFP-N1 (BD Biosciences Clontech, Palo Alto, California) by electroporation (Bio-Rad Model GenePulser^{TM}, Hercules, California; 220 V, 960 μ Fd, ∞Ω) or transduced with a human immunodeficiency virus type 1 (HIV-1)-based, lentiviral vector system constitutively expressing enhanced GFP (20,21). For the lentivirus, the GFP coding sequence was inserted into the vector 5-prime of the internal ribosome entry site and puromycin sequences, each of which were under control of the early cytomegalovirus promoter. Infectious stocks were prepared by transfection of 293T cells and used at a multiplicity of infection of ~10.

The origin of MDA-MB-435 has been questioned since the cells express melanoma-associated genes in cDNA microarray experiments {27157}. However, the patient was reported only to have a breast carcinoma. Since MDA-MB-435 cells express milk proteins (22), it is most simple to conclude that the cells are poorly differentiated breast carcinoma.

Parental cells were cultured in a mixture (1:1 *v:v*) of Dulbecco's modified Eagle's medium and Ham's F12 media (DMEM/F12; Invitrogen, Carlsbad, CA) supplemented with 2 mM L-glutamine, 1 mM sodium pyruvate, 0.02 mM non-essential amino acids, 5% fetal bovine serum (Atlanta Biologicals, Norcross, Georgia), without antibiotics or antimycotics (cDME/F12). All cultures were confirmed negative for *Mycoplasma spp.* infection using a PCR-based test (TaKaRa, Shiga, Japan).

GFP-expressing cells were grown in cDME/F12 plus G418 (Geneticin, 500 μg/ml, Invitrogen) or puromycin (500 μg/ml, Fisher Scientific). The brightest 15% (lentiviral) or 25% (pEGFP) fluorescing cells were sorted using either Coulter EPICS V cell sorter (Beckman-Coulter, Fullerton, California) or a BD FACSaria cell sorter (BD Biosciences Immunocytometry Systems, San Jose, California).

Intracardiac injections

Cells at 80–90% confluency were detached using a mixture of 0.5 mM EDTA and 0.05% trypsin in Ca^{+2}-, Mg^{+2}- and $NaHC0_3$- free Hank's balanced salt solution (HBSS). Viable cells were counted using a hemacytometer and resuspended at a final concentration of 1.5 x 10^6 cells/ml in ice-cold HBSS. Cells were not used unless viability was >95%, but was usually >98%. Female athymic mice aged between 4–6 wk (Harlan Sprague-Dawley, Indianapolis, IN) were anesthetized by intramuscular administration of a mixture of Ketamine-HCl (129 mg/kg), and Xylazine (4 mg/kg). Cells (3×10^5 in 0.2 ml) were injected into the left ventricle of

the heart between the 3rd and 4th or 4th and 5th intracostal space. The presence of bright red, as opposed to burgandy, colored blood prior to and at the end of each inoculation confirmed injection of the entire volume into the arterial system. Mice were necropsied at 1, 2, 4, 8, 24, 48 and 72 hr and 1, 2, 4 and 6 wk post-inoculation following anesthesia with Ketamine:Xylazine and euthanasia by cervical dislocation. At least two independent experiments were performed with 5–12 mice per experimental group. Not all time points were collected for every experiment.

Although widespread skeletal metastases develop after intracardiac injection (15,23), the experiments reported here focused exclusively on the femur, a common site for metastasis that is easily accessible. The femurs were removed and examined by low magnification (2-10X) fluorescence stereomicroscopy and histological and histomorphometric analysis (24,25). Some femurs were divided into proximal and distal metaphyses plus cortical shaft (diaphysis) from which the marrow was collected and cells examined by flow cytometry or quantitative real-time PCR. Corroborating experiments were done with the contralateral femur to assure that there was not a bias for sidedness.

Mice were maintained under the guidelines of the National Institutes of Health, the University of Alabama at Birmingham and the Pennsylvania State University. All protocols were approved and monitored by the appropriate Institutional Animal Care and Use Committees.

Fluorescence microscopy

To visualize metastases derived from the GFP-tagged cell lines, whole femurs (dissected free of soft tissue using a #11 scalpel blade with gauze used to grip and remove tissue remnants) were placed into petri dishes containing ice-cold Ca^{+2}- and Mg^{+2}-free Dulbecco's phosphate-buffered saline (CMF-DPBS) and examined by fluorescence microscopy utilizing a Leica MZFLIII dissecting microscope with 0.5X objective and GFP fluorescence filters ($\lambda_{excitation}$ = 480 ± 20 nm, $\lambda_{emission}$, 510 nm barrier; Leica, Deerfield, Illinois). Photomicrographs were collected using a MagnaFire™ digital camera (Optronics, Goleta, California), and ImagePro Plus 5.1 software (Media Cybernetics, Silver Spring, Maryland).

Bone fixation and storage

Intact, dissected femurs from individual mice were placed in 25-ml glass scintillation vials and fixed in freshly prepared 4% paraformaldehyde in CMF-DPBS or in periodate-lysine-paraformaldehyde solution (26) at 4°C for 24 – 48 hr. GFP fluorescence was difficult to maintain in fixed tissues and bone sections; however, we were able to overcome this limitation by maintaining the samples at 4°C (27). Bones destined for histological sectioning were subsequently removed and decalcified in 0.5 M EDTA in CMF-DPBS.

Bone Histomorphometry

Bones were dehydrated in increasing concentrations of ethanol and embedded in a mixture of 80:20 methyl methacrylate and dibutylphthalate. Serial coronal sections (5 μm) were obtained using a Leica 2265 microtome. The distal ends of femurs (spongiosa) were analyzed. Sections were first stained with Sanderson's Rapid Bone Stain for 2 min. Once tumor cells were identified, subsequent sections were stained with Goldner's trichrome and tartrate resistant acid phosphatase (TRAP). Histomorphometry was performed at the UAB Center for Metabolic Bone Disease Histomorphometry and Molecular Analysis Core Facility by the method of Parfitt *et al.* (24,25) using Bioquant image analysis software (R & M Biometrics, Nashville, TN).

Immunohistochemistry

Paraffin-embedded samples were sectioned (5 μm, coronal or sagittal), deparaffinized and rehydrated before antigen retrieval by microwaving for approximately 8 min at full power (700 watt) in a 10 mM citrate buffer, pH 6. Samples were boiled for 5 min in the microwave oven. Endogenous peroxidase activity was blocked by treatment with 3% hydrogen peroxide for 5 min. Sections were blocked with 1% goat serum for 1 hr. Slides were incubated with primary rabbit polyclonal anti-GFP IgG (1:250; Cat. No. 6455, Molecular Probes, Eugene, OR) for 1 hr, followed by secondary biotinylated anti-rabbit antibody (TITRE; Level2 Ultra Streptavidin Detection System, Signet Labs, Dedham, MA). Detection was achieved using Biogenex liquid DAB kit (Biogenex, San Ramon,CA) and slides were counterstained using hematoxylin. GFP-positive tumor samples served as positive controls. Negative controls were performed by omitting the primary antibody.

Some femurs were fixed in a solution of 2% paraformaldehyde containing 0.075 M lysine and 0.01 M sodium periodate, pH 7.4, 4°C for 24 hours in an attempt to maintain alkaline phosphatase activity (26). Although the alkaline phosphatase activity was not well preserved, fluorescence was maintained; fluorescent MDA-435^{GFP} cells could be observed in femurs taken throughout the time course. Following decalcification as described above, the bones were embedded in paraffin. Paraffin embedded bones were sectioned lengthwise into 10 μm sections and several sections throughout the bone were analyzed. The sections were deparaffinized, rehydrated and stained for apoptotic cells with a modified TUNEL procedure utilizing Cy-5 rather than FITC-labeled dUTP (28). Bone sections were first scanned at 20X magnification using a fluorescence confocal microscope. Areas in which GFP positive cells were detected were further analyzed at 40X magnification with both fluorescence and phase microscopy. Fluorescent images were captured at two wavelengths $\lambda_{excitation} = 480 \pm 20$ nm, $\lambda_{emission}$, 520 nm for GFP; $\lambda_{excitation} = 647$ nm, $\lambda_{emission}$, 670 nm for Cy-5. A comparison of the numbers of breast cancer cells detected by fluorescence microscopy versus use of anti-GFP gave essentially the same trends (data not shown).

Tartrate-resistant acid phosphatase- (TRAP) positive cells were determined in femurs of mice at various times following inoculation with metastatic breast cancer cells. Two to eight sections from 2–4 bones per time were stained for the presence of TRAP by immunohistochemistry (Sigma-Aldrich). After staining, the sections were viewed with a fluorescent light microscope at 20X magnification. Three images (1349 pixels per 500 μm) from the distal end and three from the proximal end were collected and converted into JPEG format. The number of TRAP positive cells was counted in each image. The Image J program (NIH) was used to calculate the bone area in each field.

Some decalcified femurs were cryosectioned and stained for alkaline phosphatase activity (Sigma-Aldrich). The sections were examined with a light microscope, the images digitally collected, and analyzed for the amount of alkaline phosphatase stain per area of bone at the growth plate and in the trabecular region. The data were calculated as ratio of the mm^2 of the alkaline phosphatase stain to mm^2 of bone.

Flow cytometric and DNA analysis

Femurs were removed from 5–6 mice at each time and cut into the distal and proximal metaphyses and the diaphysis. Bone marrow was flushed from these regions with a 1 cc tuberculin syringe fitted with 26 gauge needle. The marrow in the center of the diaphysis was collected separately from the endosteal marrow close to the cortical bone as previously described (29). For flow cytometry, the red blood cells were lysed with ACK solution (15 mM NH_4Cl, 1 mM $KHCO_3$, 0.1 mM Na_2 EDTA) and the remaining cells fixed with 2% paraformaldehyde. Samples were stored at 4°C until they were analyzed by flow cytometry

(Coulter XL-MCL) using standardized fluorescent beads (Spherotech, Sphero™ AccuCount Rainbow Fluorescent particles, 10 μm) to estimate the total cancer cells present. Standard curves were also generated by adding known numbers of MDA-MB-435 cells to mouse bone marrow cells. The samples of the mixtures of cells were prepared in the same way as the experimental samples. A background value of 200 cells was determined from the data obtained from the control animals in which no GFP-positive cells were present.

For DNA analysis, marrow was centrifuged and frozen in CMF-DPBS. At a later time, DNA was prepared from the samples with a DNeasy kit (Qiagen). The DNA was subjected to quantitative real-time PCR (Nucleic Acid Facility, Penn State) using primers to detect the HERVK gene (human endogenous retrovirus, group K), a gene found in the human genome but not the mouse (30). To establish a standard curve, MDA-MB-435^{GFP} cells were counted, diluted and added to preparations of mouse bone marrow cells. DNA was isolated from these samples and treated as the experimental samples for PCR. Although one cell could be detected in the standard curve samples, a more conservative cut-off of 150 cells was used due to practical considerations, i.e., cell extract volumes and variations in the amount of mouse DNA present in each sample.

Statistics

Each series of injections involved between 5–15 mice per experimental group or time. Femurs were apportioned for various subsequent analyses. Comparisons between groups were done by one-way analysis of variance with Student-Neumann-Kuels or Tukey's post-tests. Statistical significance was defined as a probability $p \leq 0.05$.

Results

Kinetics of MDA-435^{GFP} tumor cells trafficking in the bone

Numerous solitary fluorescent cells could be visualized in the intact bone (i.e., the bone is not cut, but has been stripped of surrounding muscle) one hr following intracardiac injection using fluorescence microscopy (Figure 1-A1). The majority (>90%) of cells were found in the metaphyseal regions, not in the diaphysis, by fluorescence. Routine identification of single tumor cells using hematoxylin and eosin stain, while possible, proved difficult. Even with evidence that tumor cells were present in the bone (i.e., by fluorescence), we could not always unambiguously identify single tumor cells in histologic sections stained by hematoxylin and eosin (H&E).

To facilitate detection of solitary tumor cells by histology and to determine their positions within the trabeculae, cellular location was estimated in two dimensions using fluorescence. Then, serial histologic sections were cut from the regions exhibiting fluorescence. While this manipulation increased the odds of finding sections containing single cells, it was not always possible to detect cells in every 5–10 μm section stained using anti-GFP antisera. Nonetheless, as implied by the fluorescence data, most tumor cells were located in the primary spongiosa of the metaphysis of the distal femur (Figures 1- B and E panels). Although fluorescent cells were not frequently detected in the femoral head at 1 hr post-injection, some GFP-positive cells were detected by immunohistochemistry (data not shown). There was no evidence of unusual inflammation or immune cell infiltration at the sites of tumor cell arrest or colonization.

In a third, parallel approach, we detected cells without visualization constraints or sampling errors associated with sectioning, instead quantifying tumor cells in various marrow compartments using flow cytometry or real-time PCR. Separation of the marrow metaphyses and diaphysis followed by flow cytometry or real-time PCR to detect MDA-435^{GFP} cells revealed a slightly different pattern of tumor cell distribution within the bone at the early times,

but an entirely consistent pattern of distribution at the later times (Figure 2). These methods were limited because precise separation of the diaphysis from the metaphysis was not consistent. Therefore, cancer cells at the interface between bone regions could not be localized with certainty. Histologic sections confirmed precise localization (Figure 1). As a whole, the various methods to assess localization were largely confirmatory. In addition, we also determined that cancer cells in the diaphysis were mostly located next to the endosteal bone rather than in the marrow in the center of the shaft. By 4–6 wk, >95% of tumor cells were found in the endosteal marrow (Figure 5).

Of the 3 x 10^5 cells injected per mouse, a small fraction were detectable in the femurs (Table 1) as expected, since cells are distributed throughout the body following injection into the arterial circulation. Flow cytometry and real-time PCR were utilized to quantify the number of cells present. Cells were flushed from the marrow space in from the metaphyseal and diaphyseal regions and examined by flow cytometry to detect GFP-tagged cells (Figure 2). In addition, DNA isolated from the bone marrow was analyzed for the presence of human DNA by real-time PCR using a human-specific primer/probe set (Figure 2). Regardless of the method, seeding of the femurs with breast cancer cells was rare (44 ± 6 cells; 0.01% per femur and Table 1). As a result, the absolute numbers were highly variable between mice and between techniques. Thus, the total number of single cells identified was not sufficient to perform statistical analyses with adequate power. Nonetheless, we did observe several consistent changes. First, solitary cells in the diaphysis were seldom detected beyond 24 hr in any of the mice, until metaphyseal lesions had apparently extended into the diaphyses at later times (Figures 1G and 2). Second, the number of fluorescent foci (i.e., cell masses) detected by fluorescent stereomicroscopy decreased progressively from 1 hr to 72 hr. This result is consistent with clearance of disseminated tumor cells from other organs (31,32). Third, single cells persisted in the femur for up to 72 hr. In general, evidence of cell division prior to 72 hr post-inoculation was infrequent.

While initial proliferation of arrested cells was delayed, distinct metastatic foci (5 ± 1) were easily detected by fluorescence microscopy of the intact bone (Figure 1A2) as well as immunohistochemistry in the femur at 1 wk (Figure 1B2) and fluorescence microscopy of bone sections (Figure 1, E Panels). Most of the foci were small and consisted of <10 cells (i.e., only 3–4 cell divisions). Although most metastatic lesions were localized at the distal end, a fraction of the bones had fluorescent foci growing at the proximal ends as well.

By 2 weeks, larger but fewer foci (2.8 ± 0.5) were detected at the distal end (Figure 1A3 and 1B3). The foci were comprised of clusters of ~50 cells. These progressively increased in size and decreased in number to an average of 1 metastatic focus at 4 wk, presumably by coalescence (Figures 1A4, 1B4 and 1G). By 6 wk, tumor cells directly extended into the diaphysis and in some cases the whole medullary canal was occupied by tumor. Histomorphometry of the lesions revealed loss of most trabecular bone by 4–6 wk (compare Figure 1D to 1C).

Tumor cell modification of the bone microenvironment

Histomorphometric analysis further showed specific modification of the microenvironment when tumor cells were present (Figure 3). We had previously shown that MDA-435^{GFP} cells form radiographically detectable osteolytic lesions within 4–6 wk following intracardiac injection (15). That finding was corroborated by histomorphometry showing calcified bone volume decreased as tumor volume increased (Figure 3A). A decrease of 97% in the ratio of osteoid surface to bone surface (OS/BS) at 4 wk points to osteoblast loss or loss-of-function as a major contributor to the decrease in calcified bone volume. This finding is consistent with previous work showing that MDA-MB-435 and MDA-MB-231 cells induce osteoblast apoptosis (33) and retard osteoblast differentiation (34) *in vitro*.

Importantly, osteoblast number per trabecular bone surface area in the metastatic lesions decreased with time (Figure 3B). Bones from uninjected, age-matched mice served as negative controls. By 2 wk, the number of osteoblasts decreased by ~20% in tumor-bearing mice. By 4 wk, however, the decrease was more dramatic (~92% decrease)(Figure 3B). The decrease in osteoblast number was accompanied by an increase in the number of apoptotic osteoblasts observed by TUNEL (Figures 3D, 3G and 4A). Apoptotic osteoblasts were found at both proximal and distal ends of the femur, but little change in the number of apoptotic osteoblasts was observed in the diaphysis until tumor cells were routinely observed in that portion of the bone (Figure 4A). This finding suggested that osteoblast apoptosis was occurring mostly when tumor cells were present. Supporting this hypothesis, TUNEL-positive osteoblasts were found almost exclusively in the presence (≤ 50 μm) of GFP-positive breast cancer cells (Figures 3G and 4B). Previous (33) and current experiments (data not shown) have shown almost no tumor cell apoptosis when adjacent to osteoblasts. Bone sections stained for alkaline phosphatase, a marker for osteoblasts, showed a dramatic decrease as tumor burden increased (Figures 3H-J). The ratio of the area occupied by alkaline phosphatase-positive cells per area of trabecular bone in the femurs of cancer-bearing mice was significantly lower compared to healthy mice (2.0 ± 0.6 *vs*. 9.6 ± 1.7, respectively; $p \leq 0.0001$). In contrast, alkaline phosphatase activity in chondrocytes located in the growth plate was not significantly different (control = 25.9 ± 4.7; tumor-bearing = 24.1 ± 5.0).

The number of osteoclasts remained unchanged at 2 wk, but unexpectedly, a consistent decrease (~35–40%; or to 60% of control) in osteoclast number was observed at later times (Figure 3C). This difference was evident by both quantitative histomorphometric analysis (Figures 3C) and TRAP staining (Figure 3E and 3F). The absolute number of both cell populations decreased so that the ratio of osteoblasts to osteoclasts decreased from an average of forty (40) to only four (4) by 4 wk.

Discussion

Bone is the most common site for metastases from breast carcinomas and their sequella account for approximately two-thirds of the costs associated with treating women with the disease (4, 35). As with most metastases, symptoms occur relatively late in disease progression. And while prevention of metastases altogether is ideal, restriction of progression to an asymptomatic state would improve clinical management of breast cancer. Likewise, repair of already existing lesions would benefit patients whose disease progression has been halted. As a result, understanding the antecedent steps for bone metastasis and osteolysis should provide insights for developing therapeutic interventions.

The results presented here are, to the best of our knowledge, the first to describe the behavior of breast cancer cells at the earliest times after they have arrived in the femur. While the femur may not represent the behavior of tumor cells in all bones, it is a common site of secondary colonization both in breast cancer patients and experimental models. Therefore, we considered it an appropriate site for studying the process.

Single tumor cells were detected in the femur 1 hr after introduction into the arterial circulation (Figure 5B). It is noteworthy that, even at this early time, tumor cells arrested primarily in the metaphyses rather than diaphyses. While it is possible that differential expression of adhesion molecules may be found in metaphyseal *vs*. diaphyseal bone vasculature (reviewed in (36)), anatomical and physiological mechanisms also likely to be important factors. Approximately 90% of the blood flow goes to the metaphyseal regions while a smaller fraction is found in the diaphyses (reviewed in (37)). Additionally, blood flow in the diaphysis is still largely vessel-based, while in the metaphyses it is more sinusoidal. In the sinusoids, the rate of blood flow is less than 10% of that found in capillaries or other vessels (reviewed in (36)). Because of the

sluggish blood flow, weaker adhesion molecules would be not as subject to negative selection as when cells experience stronger sheer forces. Yet, arrest is not the only parameter involved. The relatively rare cells initially seeding the diaphysis fail to remain there for prolonged periods. It is also possible that cancer cells follow a gradient of growth factors or cytokines. We have preliminary evidence (A.M. Mastro *et al.* unpublished) that several cytokines are found at much greater concentrations in the metaphysis compared to the diaphysis. The limitations of the present study cannot discriminate between loss of tumor cells to immune killing, apoptosis, sheer forces, etc. *vs.* migration of tumor cells from the diaphysis to the metaphysis.

The earliest arriving tumor cells were mostly located in close proximity to osteoblasts and bone lining cells (Figure 1B). In general, although the animal-to-animal variability was considerable, the majority of cells tended to be in the endosteal marrow, rather than in central marrow (Figure 5G), suggesting that traversal from the sinusoids to trabecular space occurs relatively rapidly. This pattern is similar to that reported for hematopoietic precursors in bone marrow (29). Regardless of intra-osseous location, the trend was for tumor cell numbers to decline during the first 72 hr after arrival (Figure 5C and 5D).

It was somewhat surprising to find that most tumor cells had not begun to proliferate within 72 hr since proliferation typically begins much sooner (i.e., <48 hr) in lungs and orthotopic sites (unpublished observations). The period of quiescence or dormancy could be relevant because recent clinical studies have shown that 20–100% of women with breast cancer have evidence of disseminated tumor cells in the skeleton (38–40). Disseminated occult tumor cells within bone are thought to be in a sanctuary from which tertiary metastases could form and are thought to be responsible for late (sometimes months or years) recurrences. Based upon abundant evidence from multiple experimental models, the fraction of disseminated cells progressing to overt metastasis is small. However, the presence of disseminated cells predicts poor prognosis in many tumor types, emphasizing that their presence at non-orthotopic sites should not be ignored (38,39).

What triggers the conversion from dormant to proliferative cells remains unknown and is the subject of intense current investigation. The data presented here do not clarify the mechanistic issue, except to note that there is a substantial delay (72 hr) before the breast carcinoma cells begin to divide. Perhaps, during that time, tumor cells are altering the microenvironment. At our limits of detection, we could not tell whether there was balanced division (i.e., ½ of progeny died or were eliminated) or whether tumor cells were adapting to the bone microenvironment prior to initiating growth. Upon arriving at a secondary site, tumor cells may remain dormant, undergo a limited number of cell divisions or continue proliferating to form an overt mass. Presumably, the decisions are based upon response to signal(s) from the local microenvironment. There are self-evident cues that the tissue environment controls development of bone metastasis based upon the patterns of metastasis observed — e.g., metaphyseal > diaphyseal; distal > proximal; endosteal marrow > central marrow. The findings support and extend Stephen Paget's Seed and Soil hypothesis, by which he explains the predilection of breast carcinomas to colonize bone over other tissues (41). In short, Paget posited that tumor cells (seeds) were best suited for growth only in certain tissues (soils). The data presented here indicate that the soil may differ even within individual bones. Indeed the patterns of clinical bone metastases show marked preference for proximal and trabecular bone compared to distal or cortical bone (4). Surprisingly, the metastases arising from injection of MDA-435^{GFP} cells showed the opposite pattern – a slight, but consistent, penchant for distal, compared to proximal, femur. The pattern was consistent regardless of the method used to detect tumor cells. So, trivial experimental parameters cannot explain why, in this model, metastases develop in the distal femur with greater frequency. One possibility invokes anatomical differences between mouse and human. Mice have extremely different gaits and

mechanical pressures on their joints. Since tumor cells are generally predisposed to colonize injured tissues, biomechanical stresses on the knees in mice could, in part, explain the difference in arrest and colonization patterns between the species.

Notwithstanding preferential arrest/adhesion and growth in the metaphyses, metastatic breast carcinoma cells can still survive and grow in the diaphyses when the metastatic lesions are large enough. This growth pattern may suggest that tumor cells renovate the bone microenvironment sufficiently to reduce (or eliminate?) negative signals or that they can induce the production of positive factors from local, non-tumor cells. Whether neoplastic cells have surpassed a threshold number, or whether some negative influence on tumor cells has been overcome, the incapacity to colonize diaphyses is not absolute.

It is widely accepted that metastatic breast carcinoma cells manipulate the bone microenvironment to induce osteolysis. In particular, tumor cell activation of osteoclasts via the 'vicious cycle' of secretion of PTHrP or RANK ligand has been implicated in bone resorption (4,19,42). However, we previously hypothesized that the balance of bone deposition and resorption could be altered as well by reducing osteoblast number or differentiation and/or activity (33). *In vitro* co-culture of metastatic human breast carcinoma cells or their conditioned media with human osteoblasts resulted in apoptosis of the osteoblasts (33). The *in vivo* data presented here extend the previous findings by demonstrating that osteoblasts in the regions colonized by MDA-435^{GFP} are also eliminated.

It is possible that changes in the ratio of osteoblasts to osteoclasts in tumor-infiltrated bone tilts the balance in favor of increasing osteoclastic activity, thereby promoting osteolysis. The dramatic decrease in osteoblasts observed by 4 wk prompted closer examination of osteoblast apoptosis at multiple times using TUNEL. The number of apoptotic osteoblasts progressively increased until later times, perhaps due to the already decreased number of osteoblasts. Interestingly, at earlier times (<4 wk) at least one tumor cell was in direct contact (≤50 μm) with each TUNEL-positive osteoblast (Figures 3E and 4B). While this finding does not prove that tumor cells directly induce apoptosis, the data are consistent with this hypothesis. We also found with *in vitro* studies that breast cancer cell conditioned medium prevented osteoblasts from differentiating as evidenced by lack of production of alkaline phosphatase, osteocalcin and bone siaoloprotein (34). In this current study, the lack of alkaline phosphatase activity (Figures 3H and 3I) may be due, in part, to failure of pre-osteoblasts to differentiate as well as apoptosis of mature osteoblasts. In either case, the outcome is the same, lack of functional osteoblasts.

Ours is the first *in vivo* evidence that tumor cells influence not only osteoclasts, as widely believed and demonstrated, but also osteoblasts. The findings may explain, in part, the failure of bisphosphonate-treated patients to repair osteolytic bone lesions (43) – i.e., if there are no osteoblasts to reconstitute the bone, the lesions will remain.

It was surprising that osteoclast numbers were dramatically reduced in late-stage bone metastasis. Perhaps it should not have been because Orr, Mundy and colleagues previously described that tumor cells themselves (i.e., in the absence of osteoclasts) could resorb bone (44,45). The published data, although somewhat controversial, and the evidence presented here leave open the possibility that further progression of osteoclast-initiated osteolysis is possible. Furthermore, previous publications have demonstrated significantly diminished osteoblast and osteoclast number in late-stage breast carcinoma metastasis to bone (46–48). Based upon heterogeneity amongst tumors for multiple parameters, molecular mechanisms of bone metastasis may vary while yielding the same end point, osteolysis.

A potential criticism of the reported work is that the findings are based upon a single cell line. Given the heterogeneity of tumors and the redundant mechanisms from which each can choose

to accomplish a given task, we are careful not to over-generalize. Nonetheless, most key observations reported here have been replicated in the MDA-MB-231 breast carcinoma model of bone metastasis. MDA-MB-231 cells form osteolytic lesions with similar distribution as those found in MDA-MB-435. With expansion of bone lesions, osteoblast numbers decrease in MDA-MB-231 as well (P.A. Phadke and D.R. Welch, unpublished observations). Assuming that the essential elements of osteolytic metastasis are observed in multiple breast carcinoma models, the findings reported here have significant implications with regard to control of bone metastasis in the clinic.

Foremost, the osteoblast is key. While tumor cells can initiate growth prior to osteolysis, one of the earliest observed changes is elimination of bone forming cells. Even if bone resorption is controlled exogenously, repair of defects is not possible. Since the structural integrity of the skeleton is critical to survival and quality of life, comprehensive treatment needs to restore bone matrix as well as limit osteolysis. By studying the trafficking of tumor cells within the bone and the impact of their presence upon normal bone physiology, insights regarding how to improve control of bone metastasis will be forthcoming. Since the submission of this manuscript, a paper (49) describing a role for Dickkopf-1 (DKK1) in a Wnt-mediated pathway in prostate cancer cell osteoblastic lesions was published. Whether breast cancer mediated osteolysis via impairment of osteoblast function is regulated by DKK1 or other components of the Wnt signaling pathway remains to be determined.

Acknowledgements

We are grateful for the support of the U.S. Army Medical Research and Materiel Command (DAMD-17-02-1-0541, DAMD-17-03-01-0584, and DAMD 17-02-1-0358) and the UAB Breast SPORE (P50-CA89019). Additional support was provided by CA87728, the National Foundation for Cancer Research - Center for Metastasis Research and the Pennsylvania Department of Health Breast Cancer Program.

We are also indebted to the superb technical assistance from Virginia R. Gilman as well as Patti Lott at the UAB-Center for Metabolic Bone Disease Histomorphometry Core Facility, UAB Breast SPORE Tissue Core Facility, Deborah Grove and the Penn State Nucleic Acid Core Facility, and the Penn State Electron Microscopy and Histology Core Facility. We appreciate the critical reading of the manuscript and helpful suggestions from Dr. Tom Clemens.

This work is submitted in partial fulfilment of the requirements for the UAB Graduate Program in Molecular and Cellular Pathology (P.A.P.) and Penn State Graduate Program in Biochemistry and Molecular Biology (R.R.M.).

References

1. Body JJ. Metastatic bone disease: clinical and therapeutic aspects. Bone 1992;13 (Suppl 1):S57–S62. [PubMed: 1581121]
2. Coleman RE. Skeletal complications of malignancy. Cancer 1997;80:1588–94. [PubMed: 9362426]
3. Coleman RE, Rubens RD. The clinical course of bone metastases from breast cancer. Br J Cancer 1987;55:61–66. [PubMed: 3814476]
4. Mundy GR. Metastasis: Metastasis to bone: causes, consequences and therapeutic opportunities. Nature Rev Cancer 2002;2:584–93. [PubMed: 12154351]
5. Lelekakis M, Moseley JM, Martin TJ, et al. A novel orthotopic model of breast cancer metastasis to bone. Clin Exptl Metastasis 1999;17:163–70. [PubMed: 10411109]
6. Chirgwin JM, Guise TA. Molecular mechanisms of tumor-bone interactions in osteolytic metastases. Crit Rev Eukaryot Gene Expr 2000;12:159–78. [PubMed: 11186331]
7. Guise TA. Parathyroid hormone-related protein and bone metastases. Cancer 1997;80:1572–80. [PubMed: 9362424]
8. Yoneda T, Sasaki A, Mundy GR. Osteolytic bone metastasis in breast cancer. Breast Cancer Res Treat 1994;32:73–84. [PubMed: 7819589]
9. Averbuch SD. New bisphosphonates in the treatment of bone metastases. Cancer 1993;72:3443–52. [PubMed: 8242577]

10. Wetterwald A, vanderPluijm G, Que I, et al. Optical Imaging of cancer metastasis to bone marrow - A mouse model of minimal residual disease. Am J Pathol 2002;160:1143–53. [PubMed: 11891210]
11. Holleran JL, Miller CJ, Culp LA. Tracking micrometastasis to multiple organs with *lacZ*-tagged CWR22R prostate carcinoma cells. J Histochem Cytochem 2000;48:643–51. [PubMed: 10769048]
12. Amhlaoibh RN, Hoegh-Andersen P, Brünner N, et al. Measurement of tumor load and distribution in a model of cancer-induced osteolysis: A necessary precaution when testing novel anti-resorptive therapies. Clin Exptl Metastasis 2004;21:65–74. [PubMed: 15065604]
13. Sung V, Cattell DA, Bueno JM, et al. Human breast cancer cell metastasis to long bone and soft organs of nude mice: A quantitative assay. Clin Exptl Metastasis 1997;15:173–83. [PubMed: 9062394]
14. Murphy BO, Joshi S, Kessinger A, Reed E, Sharp JG. A murine model of bone marrow micrometastasis in breast cancer. Clin Exptl Metastasis 2002;19:561–69. [PubMed: 12498385]
15. Harms JF, Welch DR. MDA-MB-435 human breast carcinoma metastasis to bone. Clin Exptl Metastasis 2003;20:327–34. [PubMed: 12856720]
16. Yang M, Baranov E, Jiang P, et al. Whole-body optical imaging of green fluorescent protein-expressing tumors and metastases. Proc Natl Acad Sci 2000;97:1206–11. [PubMed: 10655509]
17. Manolagas SC. Birth and death of bone cells: basic regulatory mechanisms and implications for the pathogenesis and treatment of osteoporosis. Endocrine Rev 2000;21:115–37. [PubMed: 10782361]
18. Parfitt AM. Osteonal and hemi-osteonal remodeling: the spatial and temporal framework for signal traffic in adult human bone. J Cell Biochem 1994;55:273–86. [PubMed: 7962158]
19. Roodman GD. Mechanisms of disease: Mechanisms of bone metastasis. N Engl J Med 2004;350:1655–64. [PubMed: 15084698]
20. Van Tine BA, Kappes JC, Banerjee NS, et al. Clonal selection for transcriptionally active viral oncogenes during progression to cancer. J Virol 2004;78:11172–86. [PubMed: 15452237]
21. Chen W, Wu X, Levasseur DN, et al. Lentiviral vector transduction of hematopoietic stem cells that mediate long-term reconstitution of lethally irradiated mice. Stem Cells 2000;18:352–59. [PubMed: 11007919]
22. Sellappan S, Grijalva R, Zhou XY, et al. Lineage infidelity of MDA-MB-435 cells: Expression of melanocyte proteins in a breast cancer cell line. Cancer Res 2004;64:3479–85. [PubMed: 15150101]
23. Harms JF, Welch DR, Samant RS, et al. A small molecule antagonist of the alpha-v, beta-3 integrin suppresses MDA-MB-435 skeletal metastasis. Clin Exptl Metastasis 2004;21:119–28. [PubMed: 15168729]
24. Parfitt AM. Bone histomorphometry: proposed system for standardization of nomenclature, symbols, and units. Calcif Tissue Int 1988;42:284–86. [PubMed: 3135094]
25. Parfitt AM, Drezner MK, Glorieux FH, et al. Bone histomorphometry: standardization of nomenclature, symbols, and units. Report of the ASBMR Histomorphometry Nomenclature Committee. J Bone Miner Res 1987;2:595–610. [PubMed: 3455637]
26. Miao D, Scutt A. Histochemical localization of alkaline phosphatase activity in decalcified bone and cartilage. J Histochem Cytochem 2002;50:333–40. [PubMed: 11850436]
27. Harms JF, Budgeon LR, Christensen ND, Welch DR. Maintaining green fluorescent protein tissue fluorescence through bone decalcification and long-term storage. Biotechniques 2002;33:1197–200. [PubMed: 12503297]
28. Jewell J, Mastro AM. Using terminal deoxynucleotidy transferase (TDT) enzyme to detect TUNEL-positive, GFP-expressing apoptotic cells. Applications in Cell Notes 2002;3:13–14.
29. Mason TM, Lord BI, Hendry JH. The development of spatial distributions of CFU-S and in-vitro CFC in femora of mice of different ages. Br J Haematol 1989;73:455–61. [PubMed: 2611133]
30. Mager DL, Medstrand P. Retroviral repeat sequences. In: Anonymous Encyclopedia of the Human Genome. London: Macmillan Publishers Ltd., Nature Publishing Group; 2003. p.1–7.
31. Goldberg SF, Harms JF, Quon K, Welch DR. Metastasis-suppressed C8161 melanoma cells arrest in lung but fail to proliferate. Clin Exptl Metastasis 1999;17:601–07. [PubMed: 10845559]
32. Fidler IJ. Metastasis: quantitative analysis of distribution and fate of tumor emboli labeled with ^{125}I-5-iodo-2′-deoxyuridine. J Natl Cancer Inst 1970;45:773–82. [PubMed: 5513503]

33. Mastro AM, Gay CV, Welch DR, et al. Breast cancer cells induce osteoblast apoptosis: a possible contributor to bone degradation. J Cell Biochem 2004;91:265–76. [PubMed: 14743387]
34. Mercer RR, Miyasaka C, Mastro AM. Metastatic breast cancer cells suppress osteoblast adhesion and differentiation. Clin Exptl Metastasis 2004;21:427–35. [PubMed: 15672867]
35. Lipton A. Management of bone metastases in breast cancer. Curr Treat Options Oncol 2005;6:161–71. [PubMed: 15717997]
36. Welch DR, Harms JF, Mastro AM, Gay CV. Breast cancer metastasis to bone: Evolving models and research challenges. J Musculoskel Neur Interact 2003;3:30–38.
37. Gross TS, Clemens TL. Vascular control of bone remodeling. In: Anonymous Advances in Organ Biology. JAI Press Inc.; 1998. p.138–60.
38. Pantel K, Woelfle U. Micrometastasis in breast cancer and other solid tumors. J Biol Regulat Homeostat Agent 2004;18:120–25.
39. Pantel K, Brakenhoff RH. Dissecting the metastatic cascade. Nature Rev Cancer 2004;4:448–56. [PubMed: 15170447]
40. Masuda TA, Kataoka A, Ohno S, et al. Detection of occult cancer cells in peripheral blood and bone marrow by quantitative RT-PCR assay for cytokeratin-7 in breast cancer patients. Int J Oncol 2005;26:721–30. [PubMed: 15703829]
41. Paget S. The distribution of secondary growths in cancer of the breast. Lancet 1889;1:571–73.
42. Lynch CC, Hikosaka A, Acuff HB, et al. MMP-7 promotes prostate cancer-induced osteolysis via the solubilization of RANKL. Cancer Cell 2005;7:485–96. [PubMed: 15894268]
43. Lipton A, Theriault RL, Hortobagyi GN, et al. Pamidronate prevents skeletal complications and is effective palliative treatment in women with breast carcinoma and osteolytic bone metastases - *Long term follow-up of two randomized, placebo-controlled trials*. Cancer 2000;88:1082–90. [PubMed: 10699899]
44. Eilon G, Mundy GR. Direct resorption of bone by human breast cancer cells in vitro. Nature 1978;276:726–28. [PubMed: 732878]
45. Sanchez-Sweatman OH, Orr FW, Singh G. Human metastatic prostate PC3 cell lines degrade bone using matrix metalloproteinases. Invasion Metastasis 1998;18:297–305. [PubMed: 10729774]
46. Stewart AF, Vignery A, Silverglate A, et al. Quantitative bone histomorphometry in humoral hypercalcemia of malignancy: uncoupling of bone cell activity. J Clin Endocrin Metab 1982;55:219–27.
47. Sanchez Y, Bachant J, Wang H, et al. Control of the DNA damage checkpoint by Chk1 and Rad53 protein kinases through distinct mechanisms. Science 1999;286:1166–71. [PubMed: 10550056]
48. Mundy CR, Altman AJ, Gondek MD, Bandelin JG. Direct resorption of bone by human monocytes. Science 1977;196:1109–11. [PubMed: 16343]
49. Hall CL, Bafico A, Dai J, Aaronson SA, Keller ET. Prostate cancer cells promote osteoblastic bone metastases through Wnts. Cancer Res 2005;65:7554–60. [PubMed: 16140917]

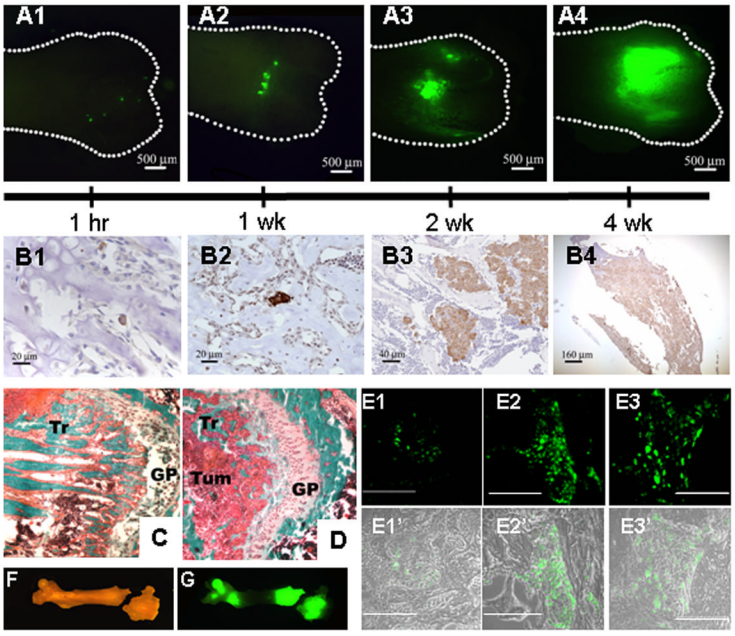

Fig 1.

The kinetics of MDA-435^{GFP} metastatic growth in the femur following intracardiac injection. Whole femurs were dissected and fluorescent foci were visualized in the intact bones using a fluorescent stereomicroscope. *Panel A*, fluorescent foci were observed, mainly in the distal end of femurs, as shown at 1 hr (A1), 1 wk (A2), 2 wk (A3), and 4 wk (A4). *Panel B*, MDA-435^{GFP} cells were detected by anti-GFP immunohistochemistry (cells stain brown) in femurs at 1 hr (B1; note: single cell), 1 wk (B2; note: clusters of 2–3 cells), 2 wk (B3), and 4 wk (B4). With time, the number of fluorescent foci decreased as the size increased. Independent tumor deposits often coalesced. *Panels C and D*, representative images of distal ends of femur stained with Goldner's trichrome stain (Panel C – normal bone, Panel D – 4 wk). The amount of trabecular bone (Tr, stained teal) is significantly lower in bone containing tumor cells, reflective of osteolytic degradation. Tumor cells (Tum) infiltrating the metaphyseal area near epiphyseal growth plate (GP) are labeled for reference. *Panel E* shows fluorescent tumor cell foci in trabecular bone in paraffin-embedded sections at 2 wk (Panel E1), 4 wk (Panel E2) and 6 wk (Panel E3) post-injection. Magnification line indicates 100 μm. Panels E1′, E2′ and E3′ are composite of fluorescent and phase images. Representative bright field (Panel F) and fluorescent (Panel G) images of a mouse femur at 4 wk show two large metastatic foci, one at each end. The distal end shows an iatrogenic fracture, presumably due to weakness caused by tumor cell-induced osteolysis.

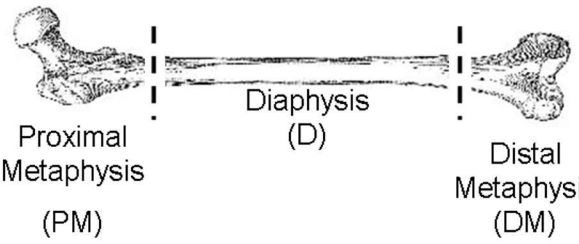

Time after injection	Flow cytometry			Real-time PCR		
	PM	D	DM	PM	D	DM
1 hr	1/5	2/5	0/5	4/5	3/5	2/5
4hr	2/5	2/5	0/5	4/5	4/5	3/5
24 hr	0/5	0/5	0/5	0/4	4/4	0/4
72 hr	2/5	1/5	2/5	2/5	4/5	1/5
1 wk	1/5	1/5	0/5	3/5	5/5	4/5
4 wk	2/5	2/5	3/5	4/5	5/5	5/5
6wk	0/3	1/3	2/3	2/3	3/3	3/3

Femoral ends were separated from the shaft with scissors. The proximal (PM) and distal (DM) metaphyses and the diaphysis (D) were flushed with ice-cold saline. Cells were collected and prepared for flow cytometry or DNA isolation and subsequent analysis by real-time PCR using HERVK, a human-specific gene. In practice, the limit of detection of MDA-435^{GFP} cells by flow cytometry was ~200 cells; by PCR it was ~150 cells. Shown are the numbers of animals in which the cancer cells were detected at various times and the bone areas in which they were found. The denominator is the number of bones examined at each time. Please note: the data presented are incidence only. The calculated number of cells is presented in Table 1 for each time.

Fig. 2.

Detection of MDA-435^{GFP} metastatic cells by flow cytometry or real-time, quantitative PCR in the metaphyseal and diaphyseal ends of the femur at various times following intracardiac inoculation.

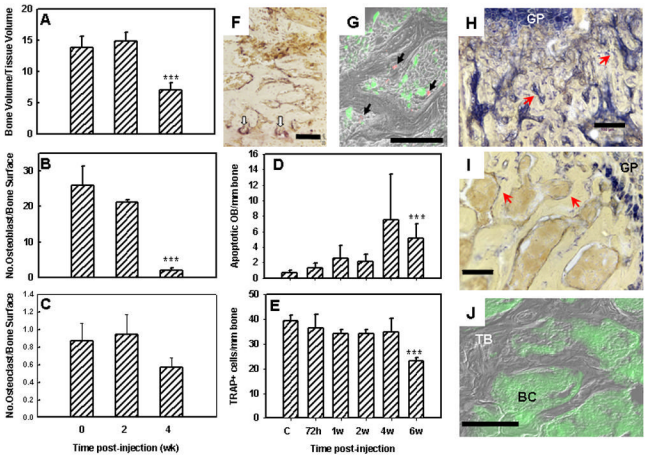

Fig. 3.

MDA-435^{GFP} breast cancer cells diminished osteoblast (OB) and osteoclast (OC) numbers in colonized bone as evaluated by quantitative bone histomorphometry, immunohistochemistry and fluorescent microscopy. *Panels A–C*, histomorphometric analyses. (*A*, Bone volume to tissue volume; *B*, Number of OB per bone surface; *C*, Number of OC per bone surface). *Panel D*, the number of apoptotic OB (TUNEL positive) per linear bone surface at times following inoculation of tumor cells. *Panel E*, the number of OC (staining for tartrate-resistant acid phosphatase, TRAP) per linear bone surface at times following inoculation of tumor cells. *Panels A–E*, *** indicates significantly different ($p \leq 0.05$) from normal bone. *Panel F*, representative image of OC staining for TRAP (red stain highlighted with white arrows) taken from a section of femur 2 wk after tumor cell inoculation. *Panel G*, merged photomicrograph of MDA-435^{GFP} tumor cells (green) surrounding apoptotic OB (red by TUNEL using Cy-5 probe) taken from a femur 6 wk following inoculation. *Panels H, I, J***,** cryosections from a femur taken 4 wk after tumor inoculation. *H,I*, stained for alkaline phosphatase activity (blue staining highlighted by red arrows) indicative of OB; *J*, merged fluorescent and phase images showing trabecular bone (TB) surrounded by MDA-435^{GFP} cells (BC). Alkaline phosphatase activity was greatly diminished in the trabecular bone of tumor-bearing femurs but was still present in the growth plate (GP). Bars = 100 μm.

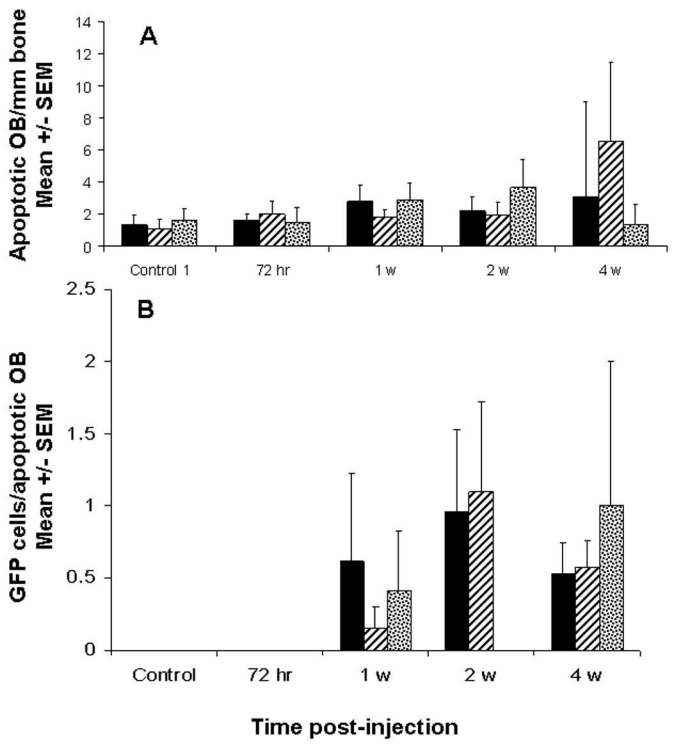

Fig. 4.

The presence of metastatic breast cancer cells in close proximity to apoptotic osteoblasts increased with time following inoculation of MDA-435^{GFP}. *Panel A*, apoptotic OB, detected by TUNEL, were counted in proximal and distal ends of paraffin sections of femur at times following tumor cell inoculation. *Panel B*, number of MDA-435^{GFP} cells within a 50 μm radius of each apoptotic OB. Shown are the averages from three femurs per time. Proximal femur (hatched); distal femur (stippled); average over femur (solid). Apoptotic osteoblasts in the diaphyses were extremely rare.

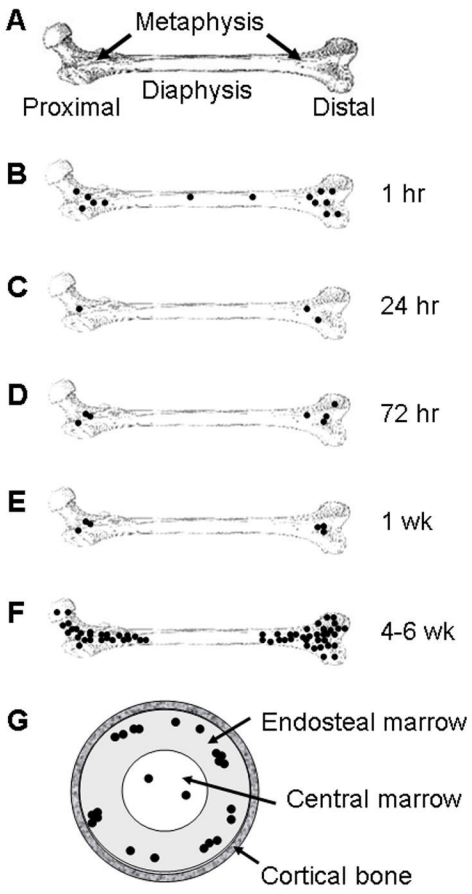

Fig. 5.

Schematic diagram depicting colonization of the femur by MDA-435^{GFP} cells. A normal femur is diagramed and labeled for reference (*Panel A*). Single cells (•) arrive in the bone marrow within 1 hr after intracardiac injection (*Panel B*), with a distribution proportionate to the relative blood flow to regions of the bone. Most cells arresting in the bone are cleared within 24 hr (*Panel C*). Of those remaining, the vast majority are still single cells but all are located in the metaphyses. A fraction of the surviving cells begin to proliferate by 72 hr (*Panel D*) with little change in the number of foci, or size of tumor cell clusters, at one week post-inoculation (*Panel E*). The lesions progressively grow in size so that by 4-6 wk, the mass of the metastases is large and the number of independently seeded cells indiscernible because the foci have coalesced. Despite not seeding and remaining in the diaphysis, metastases extend into the bone shaft as the lesions grow (*Panel F*). Flushing of bone marrow in established metastases as depicted in Figure 2, revealed that most of the tumor cells are found in endosteal marrow (~90%) or in the central marrow (~10%), but never in the cortical bone of the diaphysis, as depicted in a cross-sectional view (*Panel G*).

Table 1

Retention of MDA-435^{GFP} cells in the femur following intracardiac injection

Time post-injection	Number of MDA-435^{GFP} cells in the femur	
	Geometric Mean	± 1 Std. Dev.
1 hr	41	16; 104
4 hr	54	5; 529
24 hr	40	7; 270
72 hr	44	11; 180
1 wk	41	20; 82
4 wk	11,271	2,893; 43,915

Marrow containing tumor cells was isolated from femurs as described in Materials and Methods. The numbers of MDA-435^{GFP} cells were determined by real-time, quantitative PCR using probes for the human gene, HERVK. Shown are log-transformed data for 4–5 mice per group and only mice containing MDA-MB-435^{GFP} cells were included in the analysis.